

1 Tracking Ionospheric Changes during Solar Eclipses: Concepción

2 Historical Data

3 Adán Y. Godoy¹, Manuel A. Bravo¹, Benjamín A. Urra¹, Carlos A. Castillo-Rivera², Marayén R.
4 Canales³, Alberto J. Foppiano¹

5 ¹Centro de Instrumentación Científica, Universidad Adventista de Chile, Chillán, Ñuble, Chile

6 ²Departamento de Física, Universidad de Santiago de Chile, Estación Central, Santiago, Chile

7 ³Departamento de Geofísica, Universidad de Concepción, Concepción, Bío Bío, Chile

8 *Correspondence to:* Manuel A. Bravo (manuelbravo@unach.cl)

9 **Abstract.**

10 Solar eclipses offer a unique natural experiment to probe ionospheric responses to sudden reductions in solar radiation. **This**
11 **study reports the recovery of historical ionogram records to analyze the ionospheric response to solar eclipses spanning**
12 **several decades** over Concepción (36.79°S, 73.03°W)/Chillán (36.64°S, 71.99°W). **Out of 21 identified events between 1958**
13 **and 2024, data from 16 (76%) cases were rescued, many originally on fragile or hazardous 35 mm film, emphasizing the**
14 **scientific value of long-term datasets.** Critical frequencies (foE, foF1, foF2) and virtual heights (h'E, h'F1, h'F2/F) were
15 extracted from digitized and scaled ionograms to quantify eclipse-induced perturbations. Diurnal variations show typical
16 dips in the E- and F1-layer critical frequencies, while F2-layer responses are more complex and variable. Regression analysis
17 was performed exclusively on critical frequencies, revealing a nearly linear decrease of foE **and foF1 while the maximum**
18 **obscuration percentage of the eclipse is higher,** whereas **inconsistent behavior was observed on foF2.** High-cadence
19 observations, available for select events, provided **a significantly clearer depiction of the response to the eclipses than 1-hour**
20 **resolution historical data.** Only the 2 July 2019 and 14 December 2020 eclipse responses **had been** previously published.
21 Predictions for the 06 February 2027 eclipse indicate an expected **%ΔfoE decrease of ~28% and a %ΔfoF1 decrease of ~24%**
22 **at Chillán,** offering a timely opportunity to validate the regression models and assess predictive skill.

23 **1 Introduction**

24 Solar eclipses offer unique opportunities to understand how the ionosphere reacts when solar radiation is interrupted during
25 daylight conditions. A "small night" generated by a total solar eclipse produces disturbances in the ionosphere, both directly
26 by the suppression of incident radiation or induced by chemical and transport processes. As solar radiation decreases, the
27 electron concentration of the ionospheric layers E and F1, which mainly depend on the production and loss terms, decrease
28 considerably or even disappear throughout the eclipse. Other layers, such as the F2 layer, for which the electron

29 concentration depends significantly on plasma transport by neutral winds and electrodynamics, react with delays and are
30 difficult to predict (Le et al., 2009; Hoque et al., 2016; Zhang et al., 2024). Furthermore, the ionosphere's response depends
31 on regional conditions and external factors such as space weather and lower atmospheric coupling. Additionally, changes in
32 the virtual and real heights of ionospheric layers, such as h'F1, h'F2/F, and hmF2, have been frequently reported, generally
33 showing an upward motion followed by a post-maximum descent as the ionosphere recovers (Le et al., 2008; Chuo, 2013 ;
34 Zhang et al., 2024).

35 Historically, from 1920 onward, studies of solar eclipses have progressively revealed how reduced solar radiation affects the
36 ionosphere **and its coupled electrodynamic processes** (Mitra et al., 1933; Ratcliffe, 1956; Rishbeth, 1968). Early radio
37 observations established solar radiation as the main ionization source and highlighted layer-specific density and plasma
38 transport effects (Higgs, 1942; Evans, 1965a, 1965b). **These early eclipse experiments also contributed to the development of**
39 **ionospheric recombination theories and to the identification of characteristic temporal delays in ionospheric recovery**
40 **processes.** From 1960–2015, hundreds of studies based on observations with instruments such as **Very Low Frequency**
41 **(VLF) receivers, Global Navigation Satellite System (GNSS) arrays, ionosondes, riometers, incoherent scatter radars and**
42 **Doppler systems have determined eclipse-induced variations in Total Electron Content (TEC), critical frequency (foF2) and**
43 **height of the maximum electron density of the F2 layer (hmF2), electron temperature, and ion velocities** (Cheng et al., 1992;
44 **Afraimovich et al., 2002; Jakowski et al., 2008; Le et al., 2008; Momani et al., 2010; Kumar et al., 2013; Pezzopane et al.,**
45 **2015). These studies have consistently shown that during eclipses there are delayed responses, latitude-dependent effects,**
46 **and evidence of acoustic gravity waves (AGWs) and traveling ionospheric disturbances (TIDs) associated with eclipse**
47 **conditions** (Cheng et al., 1992; Jakowski et al., 2008; Kumar et al., 2013). **In several cases, eclipse-induced perturbations**
48 **were found to differ substantially between the E, F1, and F2 regions, reflecting the distinct chemical and dynamical**
49 **processes governing each ionospheric layer.** Major events like the 2017 Great American Eclipse provided unprecedented
50 high-resolution data, allowing detailed modeling and confirmation of earlier findings (Huba & Drob, 2017; Reinisch et al.,
51 2018; Lei et al., 2018; Aryal et al., 2019), while recent studies emphasize the role of geomagnetic activity and AGW
52 generation in modulating post-eclipse ionospheric dynamics. **Recent studies have also emphasized the importance of**
53 **combining long-term ionosonde records with modern GNSS observations to better characterize regional ionospheric**
54 **responses to eclipse forcing.** A detailed review of these studies is compiled in Appendix A of Bravo et al. (2020).

55 Early days determination of ionospheric responses during solar eclipses **were** made mainly from ionosonde (vertically
56 incidence HF radar) observations. There are long time series of these observations, allowing the study of ionospheric long-
57 term trends. Early works are, for example, those of Smith and King (1981), Bremer (1992), Ortiz de Adler et al. (1997),
58 Jarvis et al. (1998), Foppiano et al. (1999). Later work has been reviewed by Lastovicka et al. (2017, and references within)
59 and recent progress reported by Lastovicka (2023). One of these long-term series also offers a unique dataset to analyze both

60 short-term eclipse-induced ionospheric variations and broader temporal trends in the South American sector (Bravo et al.,
61 2020).

62 A vast historical record of ionograms is preserved on physical media, the recovery of which is essential for constructing
63 long-term time series. This information is key to conducting long-term trend studies that contribute to a better understanding
64 of the behavior and evolution of the regional ionosphere. Therefore, this work aims to demonstrate the scientific value of
65 rescuing this analog material by digitizing it and correctly extracting the relevant ionospheric parameters.

66 The purpose of this work is to characterize the response of the Concepción (36.79°S, 73.03°W)/Chillán (36.64°S, 71.99°W)
67 ionosphere under solar eclipse conditions, so that its response can be associated with parameters such as the **maximum**
68 **obscuration level** or time of day in order to predict the response for future eclipses.

69 **2 Methodology**

70 **2.1 Eclipse Event Selection and Station Characteristics**

71 A comprehensive search was conducted to identify all solar eclipse events whose trajectory passed over the ionospheric
72 observation stations in central Chile during the period 1957–2024.

73 Ionospheric characteristics during these events were selected from the long series of ionosonde records (ionogram) of
74 ionospheric station j3o: Concepción (36.79°S, 73.03°W). The Concepción ionosonde was a C4 type (1-25 MHz range) and
75 associated antennae (crossed deltas), installed in 1957 at the Universidad de Concepción, Andalien campus, by personnel
76 from the National Bureau of Standards (NBS, USA) for the International Geophysical Year (Ramírez, 1963). Later, the
77 ionosonde was moved to the nearby Bellavista campus (less than 2 km), the sweep range modified (0.25-20 MHz) and the
78 antennae improved to make better use of the quiet electromagnetic environment (adjustable folded dipole 0.25 to 3 MHz and
79 log-periodic 3 to 20 MHz). Maintenance difficulties of the antennae lead to a change during 1975 (cross deltas again). The
80 C4 ionosonde operated till 1994 with a transmitted power of approximately 1–5 kW, and employed simple pulse
81 transmissions without signal coding. Ionograms were recorded on 35 mm film. The interpretation and scaling required
82 optical projection on a screen and visual determination of parameters using a manual overlay. The j3o station resumed
83 operation in 1999. An IPS 42 type ionosonde (1- 22 MHz) was installed using the existing antennae. Recording was changed
84 from photographic to digital and routine observations were made until 2012, when it was relocated approximately 100 km
85 northeast to Chillán (36.64°S, 71.99°W), renamed as j3p, as part of an instrumentation modernization program (Ovalle et al.,
86 2017). For a short time interval a Canadian Advanced Digital Ionosonde (CADI) was also used. The ionosondes were
87 operated by dedicated academics, supported by electronic engineers and technicians (Muzzioli, 1977; Bravo et al., 2011),
88 providing continuous and high-quality measurements of ionospheric parameters (critical frequencies, virtual heights, etc.).
89 The ionosonde and antennae changes do not preclude standard accuracy of critical frequencies and virtual heights since these

90 parameters are not very system gain sensitive. Both locations share similar geomagnetic latitude characteristics, enabling the
91 construction of a long-term ionospheric database representative of the mid-latitude South American sector.

92 From the initial catalog of eclipse events identified, we selected those with solar obscuration exceeding 15% as observed
93 from the station coordinates (21 events). This threshold was established to ensure detectable ionospheric perturbations while
94 maintaining sufficient statistical samples for comparative analysis. Selected events span various phases of the solar cycle and
95 include eclipses with obscuration levels ranging from partial to near-totality, providing a diverse dataset for investigating the
96 relationship between eclipse magnitude and ionospheric response.

97 **2.2 Historical Ionogram Database**

98 Ionospheric observations analyzed in this study comprise a unique historical archive of vertical incidence ionograms
99 recorded between 1958 and 2024. The sounding cadence varied throughout the operational period, with temporal resolutions
100 of 1 hour, 30 minutes, 15 minutes, 5 minutes and 1 minute, depending on scientific objectives and operational constraints of
101 each campaign period. Higher-cadence observations (1–5 minute intervals) were typically implemented during special
102 events, including eclipse campaigns and geomagnetic storm monitoring periods.

103 The archival records consist primarily of 35 mm photographic film containing ionogram traces acquired by: C4 ionosonde
104 (1957–1994), IPS-42 system **which** delivered digital ionograms during an intermediate period (1999-2012), CADI for a few
105 days only, and IPS 42 after that. A substantial portion of this historical dataset had not been previously **scaled and** interpreted
106 or had undergone only partial manual scaling, representing a significant untapped scientific resource for long-term
107 ionospheric studies.

108 **2.3 Data Processing Pipeline**

109 *2.3.1 Digitization: SOCIO Software*

110 Ionograms preserved on celluloid film were digitized using an Epson Perfection V600 Photo scanner at 1200 dpi resolution
111 to ensure adequate capture of trace details and frequency-height grid specifications. The digitized images required geometric
112 correction due to perspective distortion, film degradation, and variations in original recording formats across different
113 ionosonde systems.

114 To address these challenges, we developed the Software de Corrección de Ionogramas (SoCio; **Urra, 2026**), a MATLAB-
115 based tool specifically designed for geometric correction and standardization of historical ionogram imagery. SoCio
116 performs automated detection of the frequency-height grid structure, applies perspective correction algorithms to compensate
117 for scanning distortions, and standardizes image dimensions according to the specific ionosonde system (C4, IPS-42, or
118 CADI) that generated each record. The software includes modules for handling common film deterioration artifacts,

119 including opaque regions, physical damage, and inconsistent image density. This preprocessing step was essential for
120 ensuring accurate subsequent parameter extraction, as uncorrected geometric distortions can introduce systematic errors in
121 frequency and height measurements.

122 2.3.2 Scaling: DISS Software Enhancement

123 Following geometric correction, ionospheric parameters were extracted using the Digitized Ionogram Scaling Software
124 (DISS v. 3.0), previously employed in eclipse observation campaigns (Bravo et al., 2020). For the present study, DISS
125 capabilities were substantially enhanced to accommodate the diversity and technical challenges of the historical dataset. Key
126 improvements included: (1) implementation of interactive trace digitization tools enabling manual extraction of frequency-
127 virtual height coordinates from user-drawn traces on the ionogram display, (2) development of selectable region-of-interest
128 functionality to isolate specific ionospheric layers for detailed analysis, (3) incorporation of adjustable frequency and height
129 calibration parameters to fine-tune the pixel-to-physical-unit conversion for each ionogram variant, and (4) integration of
130 quality control modules to identify and flag problematic traces requiring manual review.

131 These enhancements enabled DISS to handle the heterogeneous characteristics of multi-decade ionosonde observations,
132 including variations in frequency sweep ranges (typically 1–20 MHz with system-dependent upper limits), height display
133 scales (100–500 km, later extended to 1000 km for topside observations), and trace characteristics influenced by film aging
134 and storage conditions.

135 2.3.3 Parameter Extraction

136 From each scaled ionogram, we extracted the following standard ionospheric parameters: critical frequencies of the E, F1,
137 and F2 layers (f_oE , f_oF1 , f_oF2) and their corresponding virtual heights ($h'E$, $h'F1$, $h'F2/F$), according to the rules given by
138 Piggott & Rawer (1972).

139 2.4 Statistical Analysis and Eclipse Response Quantification

140 Eclipse-induced ionospheric perturbations were quantified by calculating both absolute and percentage deviations of critical
141 frequencies relative to reference day values at corresponding local times. Absolute deviations were computed as:

$$142 \quad \Delta f_oL = f_o L_{eclipse} - f_o L_{reference}$$

143 where L represents the ionospheric layer (E, F1, F2). Percentage deviations were calculated as:

$$144 \quad \% \Delta f_oL = \frac{f_o L_{eclipse} - f_o L_{reference}}{f_o L_{reference}} \times 100$$

145 Reference day values were obtained from hourly monthly median parameters for each eclipse event, selecting the median
146 value across multiple reference days to minimize day-to-day ionospheric variability. These hourly monthly medians had
147 previously scaled for the World Data Centre. When hourly monthly median values were unavailable, the previous day was
148 used as the reference condition (03-11-1994, 11-09-2007, 13-11-2012, 30-04-2022 and 02-10-2024 solar eclipses). In two
149 particular cases, neither the hourly monthly median values nor the previous day provided suitable reference conditions
150 during the eclipse interval. In these cases, the International Reference Ionosphere (IRI) 2020 model (Bilitza et al., 2022) was
151 used, specifically for foF1 during the 12-11-1966 solar eclipse and for foE during the 14-12-2020 solar eclipse.

152 When multiple measurements were available during the eclipse period (depending on the operational cadence: 1, 5, 15, 30,
153 or 60 minutes), we selected the observation closest to the time of maximum obscuration for regression analysis. Linear
154 regression analysis was performed using SciPy's linregress function from stats module (SciPy v1.17.1) to investigate the
155 functional relationship between solar obscuration percentage (independent variable, x) and ionospheric parameter deviations
156 (dependent variable, y). The regression model adopted was:

$$157 \quad y = mx + b$$

158 where m represents the sensitivity of the ionospheric parameter to eclipse magnitude (slope) and b the intercept. The
159 goodness of fit was assessed using the coefficient of determination (r^2), computed as:

$$160 \quad r^2 = 1 - \frac{\sum_{i=1}^n (y_i - \hat{y}_i)^2}{\sum_{i=1}^n (y_i - \bar{y})^2}$$

161 where y_i are observed values, \hat{y}_i are predicted values from the regression line, and \bar{y} is the mean of observed values. r^2
162 quantifies the proportion of variance in ionospheric response explained by solar obscuration, with values ranging from 0 (no
163 explanatory power) to 1 (perfect prediction). To evaluate the statistical significance of the regression, the p-value associated
164 with the slope of the model will be used, considering a significance level of $\alpha = 0.05$ to reject the null hypothesis of absence
165 of linear dependence.

166 From the initial catalog of 21 eclipse events identified over the period 1957–2024 (see Table 1), ionosonde records were
167 available for only 16 events (76%). Among these, we selected events exhibiting clear ionospheric signatures and sufficient
168 data coverage during the eclipse period. Both absolute (MHz) and percentage (%) deviations were analyzed to assess
169 whether normalization by baseline values improved the linearity of the response to the eclipse. The heterogeneous nature of
170 the dataset—comprising observations from three different ionosonde systems (C4, IPS-42, CADI) with varying temporal

171 resolutions—introduces additional variability that may affect correlation strength, particularly for parameters sensitive to
 172 instrumental characteristics.

173 **Table 1:** Timing of selected solar eclipses over Concepción/Chillán (Maximum **obscuration** >15%) from 1958 to 2030, including start,
 174 maximum, and end times **at ground level**, according to Eclipse Calculator 2.0 (Masana, 2012). **Local time (LT)** corresponds to the 75°W
 175 meridian. Adjusted F10.7 solar flux values were obtained from the Space Weather Services at Collecte Localisation Satellites (CLS,
 176 <https://spaceweather.cls.fr/>).

#	Date (DD-MM-YYYY)	Start time in Concepción (hh:mm LT)	Maximum time in Concepción (hh:mm LT)	End time in Concepción (hh:mm LT)	Maximum obscuration in Concepción/Chillán (%)	Ionospheric Station: j3o, Concepción; j3p, Chillán	Eclipse-time sampling interval	Adjusted F10.7 Solar Flux (sfu)
1	12-10-1958	16:32	17:31	18:01	95	j3o: C4, cross deltas, 1-25 MHz	5 min film	219.3
2	25-01-1963	06:02	07:04	08:14	73	j3o: C4, cross deltas, 1-25 MHz	1 hour film	72.2
3	12-11-1966	07:46	08:51	10:00	49	j3o: C4, folded dipole + logperiodic, 0.25-20 MHz	5 min film	126.3
4	11-09-1969	16:03	16:53	17:35	20	j3o: C4, folded dipole + logperiodic, 0.25-20 MHz	30 min film	119.0
5	04-01-1973	08:14	09:50	11:39	78	j3o: C4, folded dipole + logperiodic, 0.25-20 MHz	5 min film	109.3
6	03-11-1975	06:22	07:06	07:52	19	j3o	Instrument failure	73.0
7	22-08-1979	11:35	13:04	14:27	31	j3o: C4, cross deltas, 0.25-20 MHz	30 min film	223.2
8	10-08-1980	14:47	15:51	16:49	27	j3o: C4, cross deltas, 0.25-20 MHz	No data	173.5
9	04-02-1981	17:25	18:18	18:56	43	j3o: C4, cross deltas, 0.25-20 MHz	1 hour film	197.5
10	12-11-1985	07:36	08:20	09:06	17	j3o: C4, cross deltas, 0.25-20 MHz	1 hour film	74.7
11	29-03-1987	06:07	06:07	07:01	58	j3o: C4, cross deltas, 0.25-20 MHz	1 hour film	75.3
12	26-01-1990	14:30	15:28	16:22	23	j3o: C4, cross deltas, 0.25-20 MHz	1 hour film	238.8
13	03-11-1994	06:49	07:45	08:46	45	j3o: C4, cross deltas, 0.25-20 MHz	1 hour film	85.9

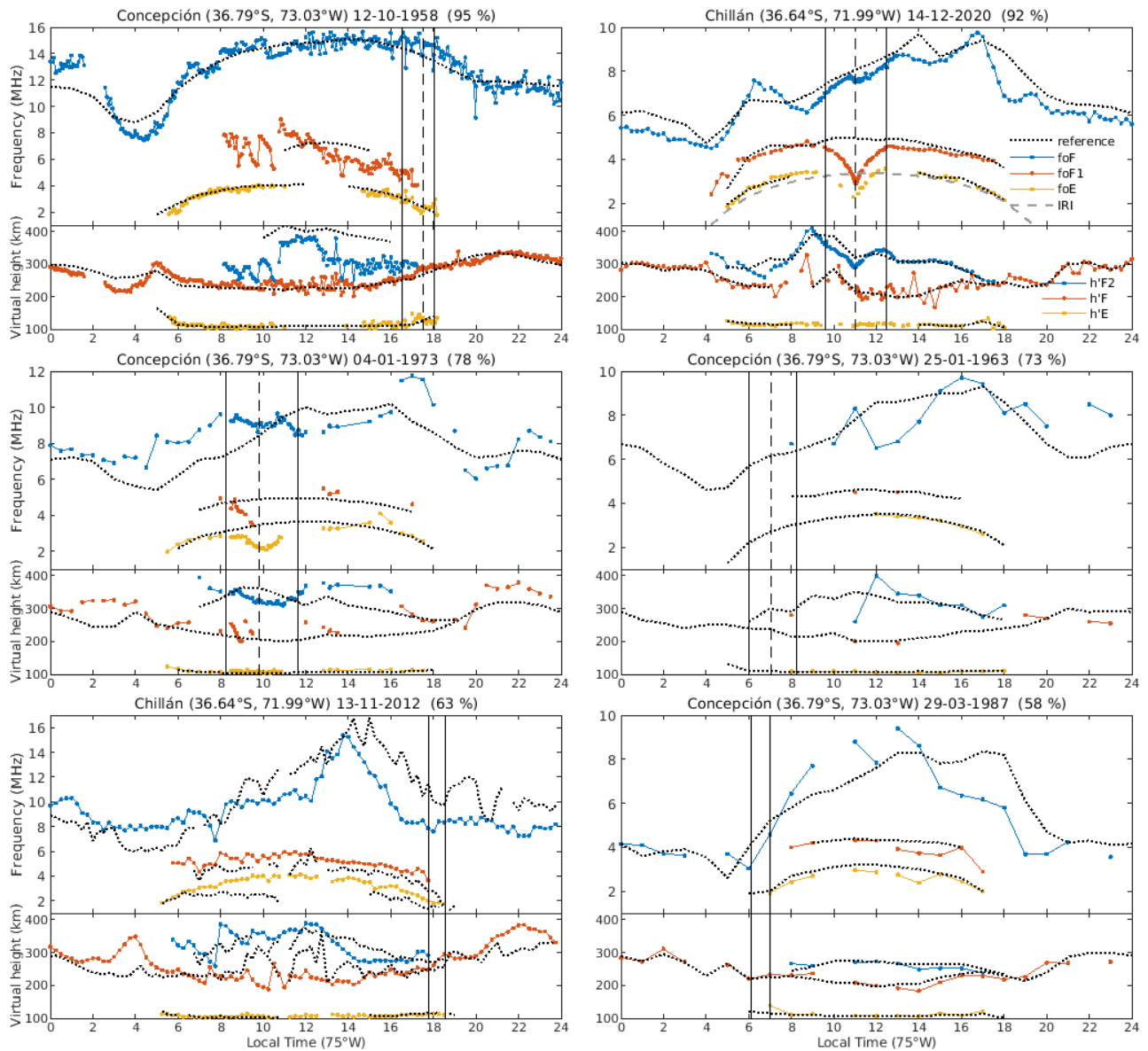
14	11-09-2007	06:03	06:46	07:55	49	j3o: IPS 42, cross deltas, 1-22 MHz	15 min digital	67.0
15	11-07-2010	14:54	15:58	16:47	62	j3o: IPS 42, cross deltas, 1-22 MHz	No data	85.4
16	13-11-2012	17:48	18:34	18:34	63	j3p: IPS 42, cross deltas, 1-22 MHz	15 min digital	143.1
17	26-02-2017	07:18	08:30	09:51	67	j3p	Instrument failure	77.5
18	02-07-2019	14:16	15:31	16:38	81	j3p	Instrument failure	69.5
19	14-12-2020	09:36	11:00	12:28	92	j3p: IPS 42, cross deltas, 1-22 MHz	1 min digital	80.4
20	30-04-2022	15:21	16:30	17:03	34	j3p: IPS 42, cross deltas, 1-22 MHz	15 min digital	121.5
21	02-10-2024	13:56	15:24	16:42	55	j3p: IPS 42, cross deltas, 1-22 MHz	5 min digital	274.8
22	06-02-2027	08:21	09:56	11:39	70	-	-	-

177

178 Using the established regression relationships, we computed predicted ionospheric responses for the upcoming 06 February
179 2027 solar eclipse, during which Chillán is expected to experience approximately 70% solar obscuration (last row of Table
180 1). These predictions are indicated by orange star markers in all regression plots, providing quantitative forecasts to support
181 observation campaign planning.

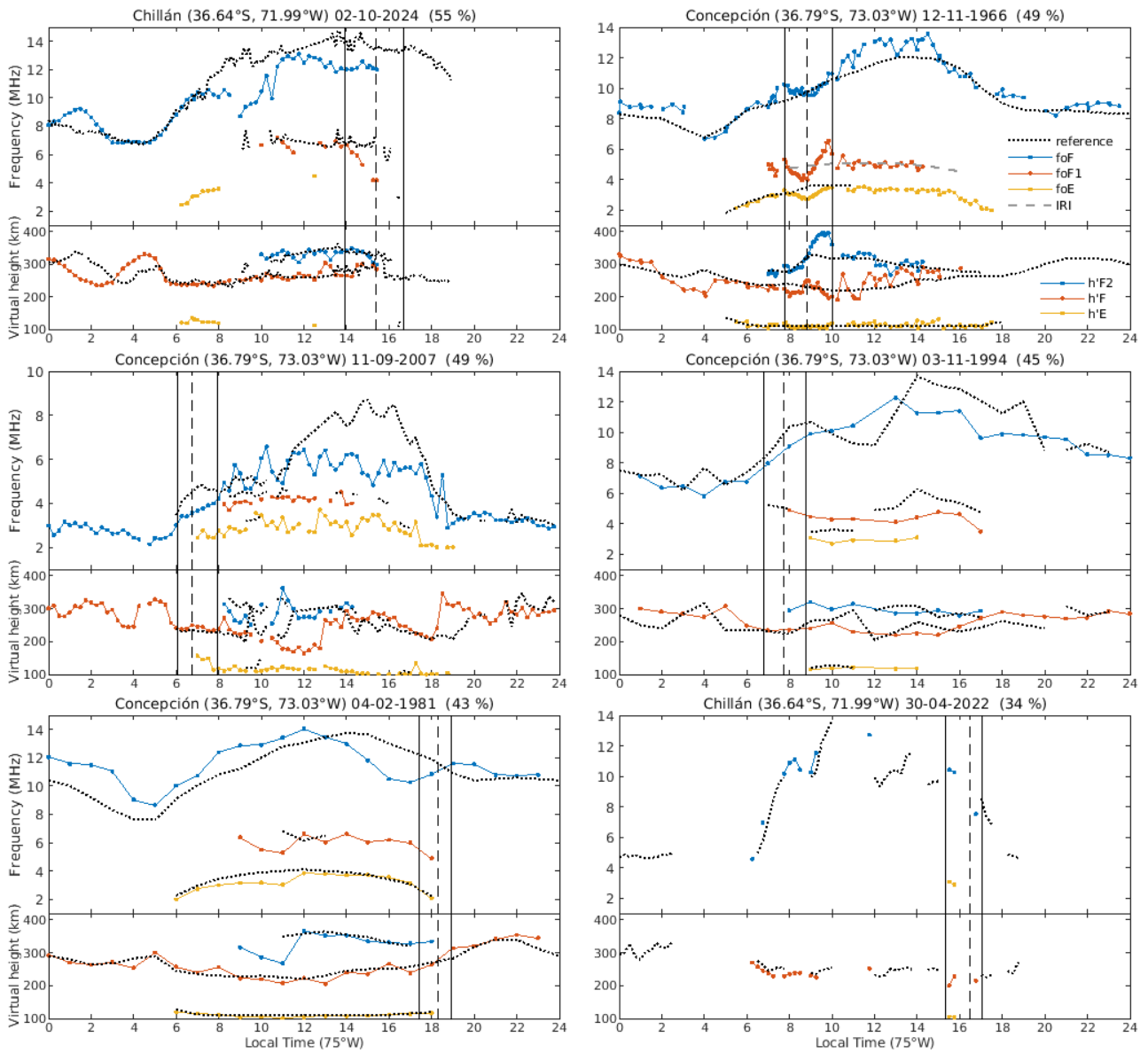
182 3 Results and Discussion

183 The diurnal variations of critical frequencies and virtual heights observed during the days in which the 16 selected eclipses
184 occur are shown in Figures 1 to 3. Reference curves are also shown for comparison. As already indicated, observed values
185 are given at different time intervals as appropriate to the available ionograms for the different eclipses. Diurnal variations are
186 arranged according to the obscuration level, regardless of the time-of-day, month, year or solar activity epoch.

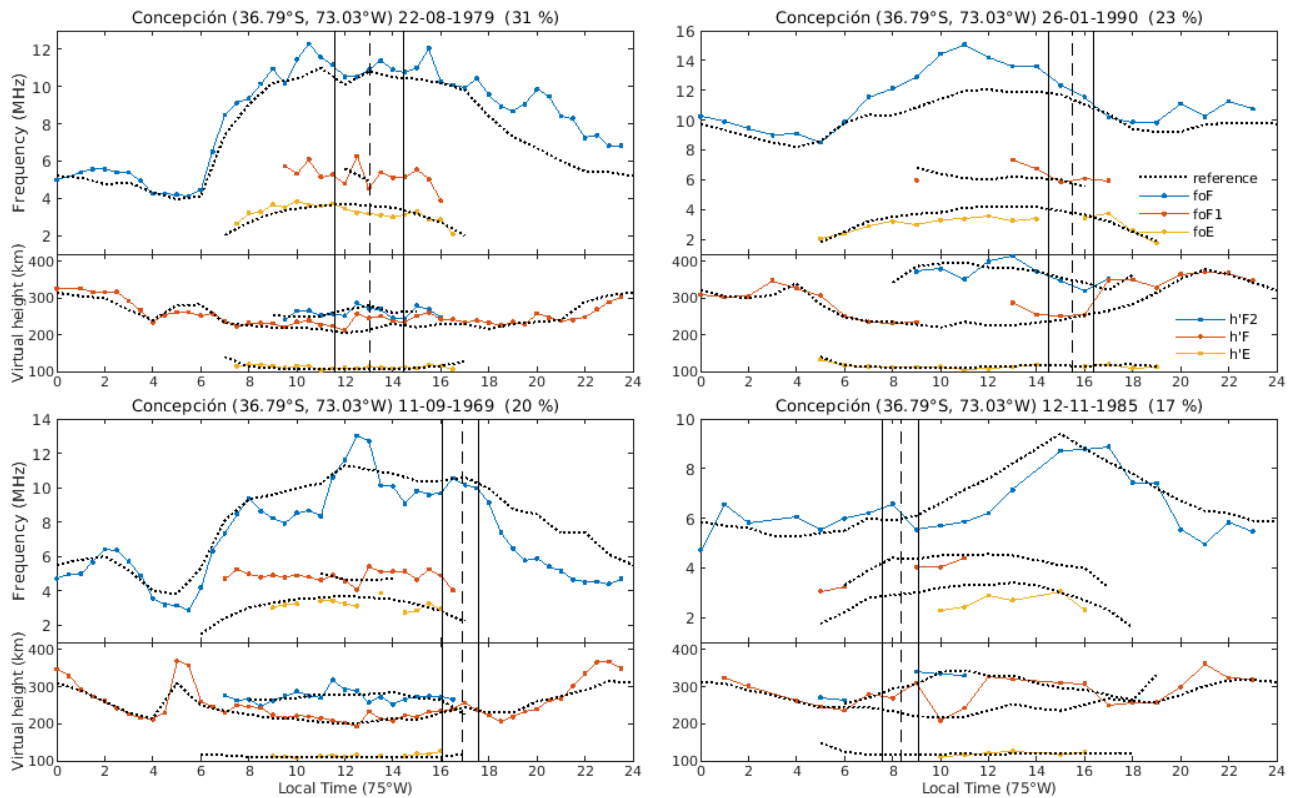


187

188 **Figure 1:** Diurnal variation of observed critical frequencies and virtual height (dots) on days of various solar eclipses with **obscuration**
 189 **levels greater than 55%** and corresponding monthly median values (dotted line). **Dates are given in DD-MM-YYYY format and the**
 190 **maximum obscuration percentage is indicated in parentheses.** Continuous vertical lines indicate onset and end of eclipse. The slash vertical
 191 line indicates the time of maximum darkness. **Note that for eclipses occurring near sunrise (sunset), the time of maximum obscuration may**
 192 **coincide with the beginning (end) of the partial solar eclipse.**



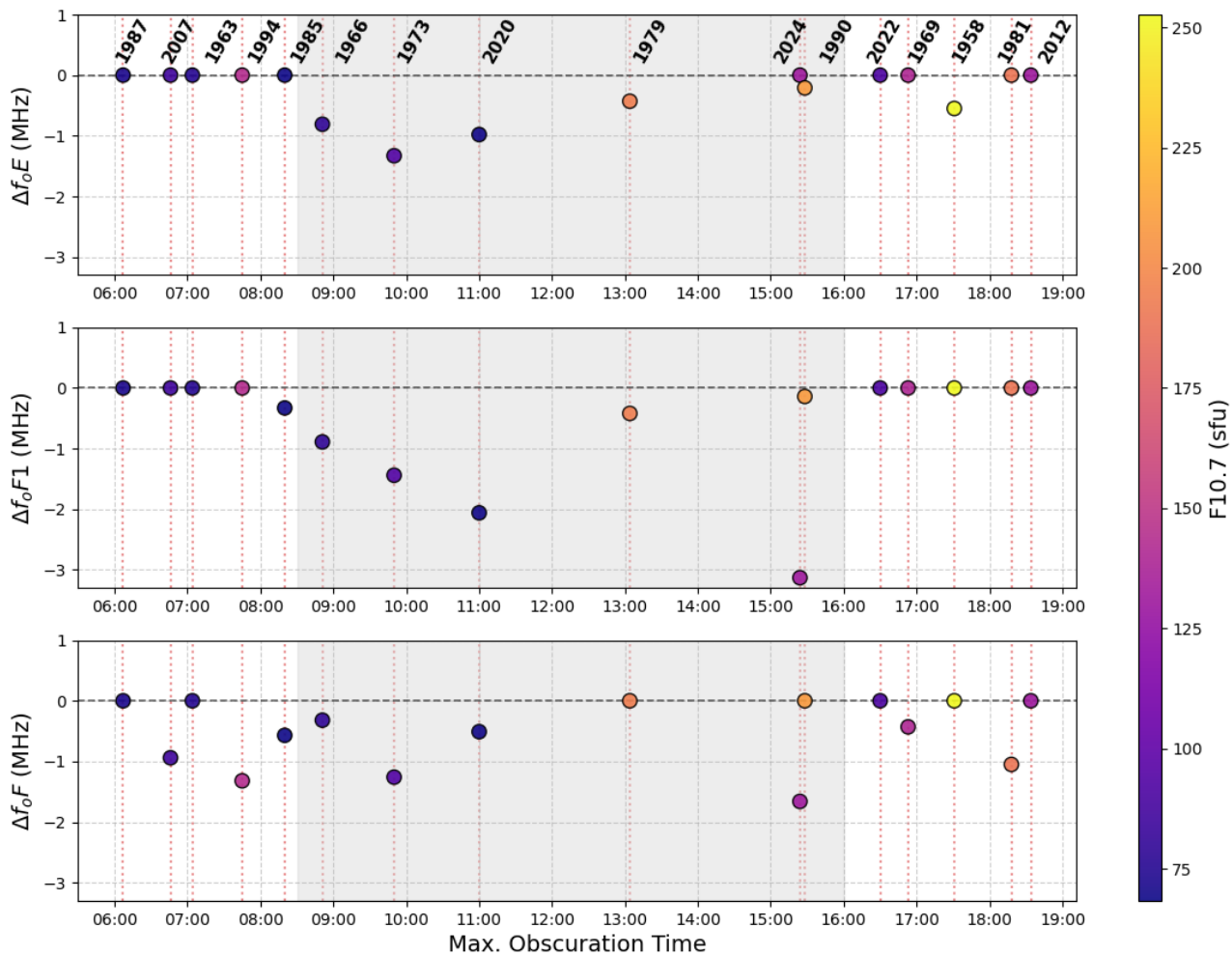
193
 194 **Figure 2:** As of Figure 1 but for **obscuration** level between 34 % and 55 %.



195
196 **Figure 3:** Same as Figure 1, but for **obscuration** level between 17 % and 31 %.

197 The clearer ionospheric effects of eclipses are seen, **as expected**, during eclipses occurring just before or around local noon.
 198 The maximum level of **obscuration** ranges from 31% to 92% for these eclipses, thus allowing to determine a fairly
 199 dependence of ionospheric effects on darkness level. The critical frequencies of the F1 and E layers show a typical dip
 200 variation, while the critical frequency of the F2 layer has more complex variations, probably showing two different stages,
 201 before and after the maximum darkness level, somehow following the variations of h'F2/F. The E layer virtual height does
 202 not seem to significantly change during these eclipses.

203 **Figure 4** presents the foE, foF1, and foF2 deviations, calculated as the difference between the minimum value observed
 204 during the eclipse interval and the corresponding reference value. The adjusted F10.7 solar flux corresponding to each event
 205 is indicated by the color scale shown in the right-hand bar. Clearer variations can be identified for foE and foF1 during
 206 specific daytime intervals, whereas the foF2 response appears less well defined. To obtain the most suitable set of
 207 differences for the linear regression analysis, only eclipse events with maximum obscuration occurring between 08:30 and
 208 16:00 LT (75°W) were selected. These correspond to six events, listed in Table 2. When no differences are observed
 209 between the reference curve and the day of the eclipse, or due to a lack of data or other reasons mentioned below, a zero
 210 value is recorded for the frequency deviations



212

213 **Figure 4:** foE, foF1, and foF2 deviations at the time of maximum obscuration for the 16 selected events. The shaded (gray) area indicates

214 the time interval in which the selected events are found (08:30 -16:00 LT). Colors indicate the adjusted F10.7 solar flux.

215 These six selected events (29%) exhibited clear ionospheric signatures and sufficient data coverage during the eclipse period
216 for the regression analysis (Figure 5). The remaining 10 events (48%) were not considered due to one or more of the
217 following limitations: (1) missing observations during critical eclipse phases (particularly around maximum obscuration), (2)
218 eclipse occurrence near sunrise or sunset when ionospheric conditions are rapidly changing, making it difficult to isolate
219 eclipse effects from diurnal variations, (3) severe film degradation preventing reliable parameter extraction despite multiple
220 scaling attempts, or (4) obscuration levels below the detection threshold for significant ionospheric perturbations. It should
221 be noted that the regression analysis was performed only on critical frequencies and not on virtual heights. Changes in virtual
222 heights ($h^{\prime}E$, $h^{\prime}F1$, $h^{\prime}F2$) were observed to be inconsistent—sometimes increasing, sometimes decreasing—making
223 prediction difficult. These variations are likely influenced by additional factors such as neutral winds, plasma transport, and
224 other dynamical processes, which complicate their response to eclipse conditions.

225

226 **Table 2:** Selected solar eclipses over Concepción/Chillán used for the linear regression analysis, including maximum obscuration at
227 ground level, according to Eclipse Calculator 2.0 (Masana, 2012). Local time (LT) corresponds to the 75°W meridian. Adjusted F10.7
228 solar flux values were obtained from the Space Weather Services at Collecte Localisation Satellites (CLS, <https://spaceweather.cls.fr/>).

229

Date (DD-MM-YYYY)	Maximum time (hh:mm LT)	Maximum obscuration (%)	Adjusted F10.7 Solar Flux (sfu)
12-11-1966	08:51	49	126.3
04-01-1973	09:50	78	109.3
22-08-1979	13:04	31	223.2
26-01-1990	15:28	23	238.8
14-12-2020	11:00	92	80.4
02-10-2024	15:24	55	274.8

230

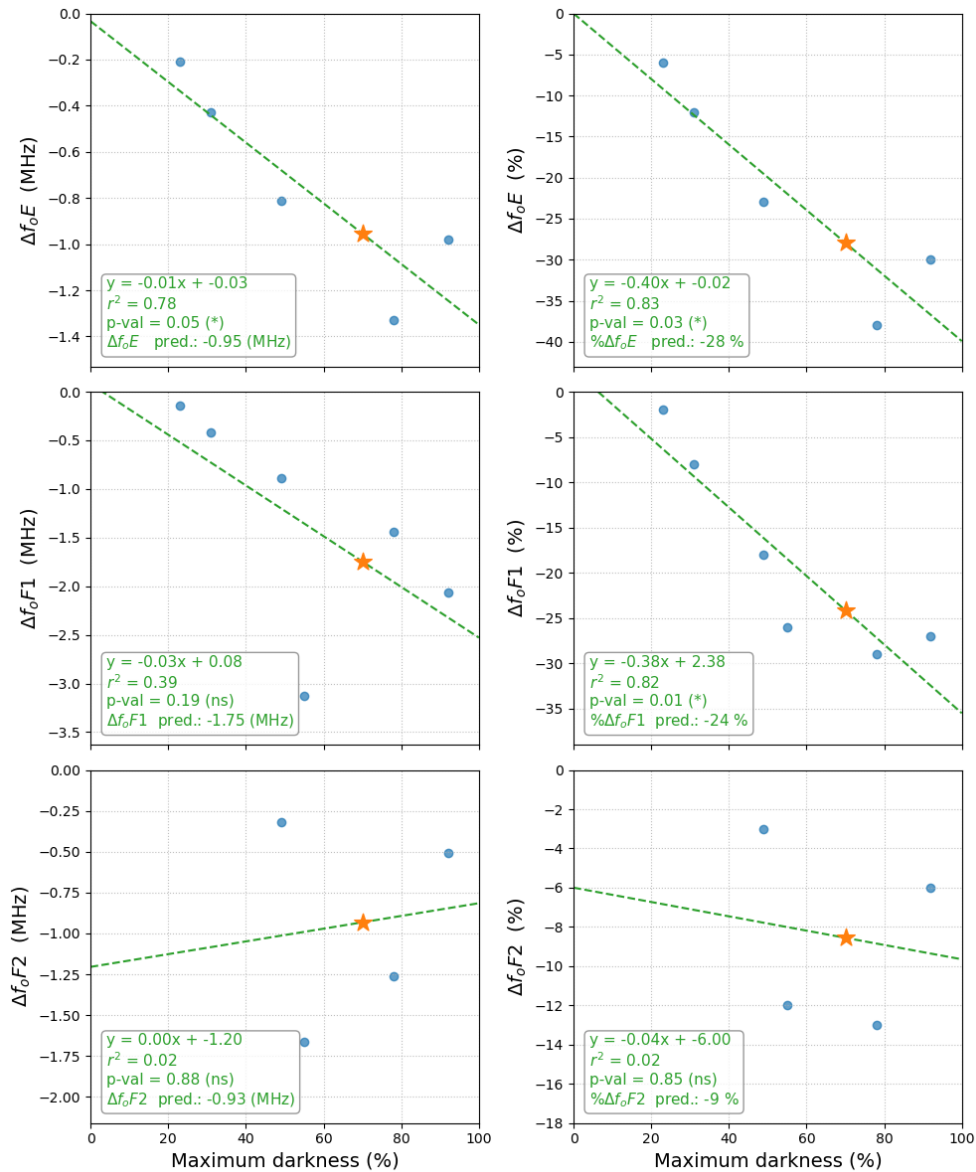
231

232

233

234

235



236

237 **Figure 5:** Linear regression analysis of ionospheric parameter deviations versus solar obscuration percentage during six eclipse events
 238 (1957–2024, blue circles). Left column: absolute frequency deviations (MHz). Right column: percentage deviations (%). Green dashed
 239 lines represent least-squares linear fits with equations, r^2 , p-value and predicted values shown. Orange stars indicate predicted responses
 240 for the 06 February 2027 eclipse (70% obscuration at Chillán).

241 Analyzing Figure 5, the E-layer critical frequency (foE) exhibited a robust linear response to solar obscuration, with absolute
 242 deviations showing the strongest correlation among all analyzed parameters ($r^2 = 0.78$, $n = 5$ events, upper left panel). The
 243 regression yielded a slope -0.01 of MHz per percent obscuration and an intercept of -0.03 MHz, indicating that foE decreases

27
28

244 nearly proportionally to eclipse magnitude. This relationship implies that a hypothetical total eclipse (100% obscuration)
245 would reduce foE by approximately 1.0 MHz relative to unperturbed reference conditions. The p-value = 0.05 is in the limit
246 of the conventional significance threshold ($\alpha = 0.05$), indicating that the relationship is statistically significant (*). In relative
247 terms (%), the relationship is even stronger ($r^2 = 0.83$, $p = 0.03$).

248 The high proportion of explained variance ($r^2 = 0.78$) reflects the rapid photochemical equilibrium characteristic of the E-
249 region, where recombination timescales (20-40 minutes) are comparable to or shorter than typical eclipse durations.
250 Consequently, E-layer ionization density responds almost instantaneously to variations in solar EUV flux, with minimal
251 influence from dynamic processes such as neutral winds or plasma diffusion that complicate interpretation of higher-altitude
252 layers.

253 When analysing foF1 response, an interesting discrepancy between absolute and relative values is observed here. In MHz,
254 the explained variance is low ($r^2 = 0.39$) and the fit is not significant ($p = 0.19$). However, when the data are normalized as
255 percentages (%), the linear relationship becomes highly significant ($r^2 = 0.82$, $p = 0.01$). This strongly suggests that the
256 dynamics of the F1 layer under an eclipse are governed more by ionization loss ratios than by absolute drops.

257 Regarding the response of the F2 layer, there is no evidence of a linear dependence on the darkening. The r^2 values are
258 practically zero (0.02) and the p values are extremely high (0.88 and 0.85). This leads to accepting (not rejecting) the null
259 hypothesis: the variation of ΔfoF2 during the analyzed eclipses appears to be dominated by external dynamic factors, such as
260 thermospheric winds or plasma transport, rather than by instantaneous local photoionization.

261 An additional source of complexity in the observed ionospheric response arises from the varying trajectories of the analyzed
262 solar eclipses. Specifically, eclipse paths that intersect the Equatorial Ionization Anomaly (EIA) region can significantly alter
263 regional electrodynamics rather than just local photochemistry. Obscuration over low latitudes reduces the E-region
264 conductivity, which subsequently weakens the equatorial $\mathbf{E} \times \mathbf{B}$ vertical drift and modulates the equatorial fountain effect
265 (e.g., Bravo et al, 2020). Consequently, this disruption in the poleward plasma transport introduces further variability in the
266 observed foF2 measurements over mid-latitude stations like Concepción/Chillán. For such events, the ionospheric depletion
267 is a complex superimposition of local photochemical loss and altered remote dynamical transport, which may explain the
268 high dispersion observed in the F2-layer data points across different eclipses.

269 Based on the established relationship, the 06 February 2027 eclipse (70% obscuration at Chillán) is predicted to induce a foE
270 reduction of 0.95 MHz (orange star, Figure 5, upper left panel). This forecast will enable direct validation of the regression
271 model and assessment of its predictive skill.

272 Several campaigns were conducted historically to obtain ionograms at higher temporal resolution during eclipses, with
273 observations every 5 minutes for significant events. However, most of these high-cadence data were never published. We

275 noted that cases with higher temporal resolution provided a significantly clearer depiction of the ionospheric response to the
276 lunar shadow, whereas 1-hour cadence datasets typically captured only one or two measurements during the obscuration
277 period. This difference in temporal resolution may affect the regression analysis, as the exact moment of maximum
278 obscuration is not always captured by the low-cadence measurements.

279 For the 2 July 2019 solar eclipse, there was a unique opportunity to measure the ionospheric response at two locations in
280 Chile: Chillán (36.64°S, 71.99°W) and La Serena (29.9°S, 71.3°W). However, the ionosonde in Chillán failed during the
281 event, so only the response at La Serena was published (Bravo et al., 2020). One of the analyzed events corresponds to the
282 14 December 2020 solar eclipse over Chillán, for which ionospheric responses were also studied by de Haro Barbas et al.
283 (2022). Their results included calculations of the alpha and beta recombination coefficients, which were found to be
284 consistent with values reported by previous authors, confirming the reliability of the ionospheric observations in this region.
285 Furthermore, prior to the 2020 eclipse, a prediction of the ionospheric response over the Chillán station had been performed
286 using the SUPIM-INPE model, estimating the expected variations in the different ionospheric layers during the event
287 (Martínez-Ledesma et al., 2020). This prediction was later validated using the observed ionospheric data, as reported in
288 Bravo et al. (2022), showing good agreement between the modeled and measured responses.

289 It is important to highlight the dedicated effort of ionosonde operators and technicians, particularly during the 1958–1994
290 period, who ensured continuous monitoring and undertook the considerable effort of recording frequent ionograms during
291 eclipses. Recovering historical data from analog ionograms stored unprocessed for decades presents a significant
292 methodological and technical challenge. The first obstacle lies in the state of preservation of the physical medium (typically
293 film reels), whose natural degradation necessitates an extremely rigorous scanning process to preserve information and
294 capture optimal contrast without damaging the medium. Subsequently, the workflow requires digital clipping to extract and
295 isolate each ionogram from the continuous record, a task that involves meticulously correcting optical and non-linear
296 distortions along the frequency and virtual height axes. Finally, parameter extraction is extremely complex: although scaling
297 systems (such as DISS software) are used, internal imperfections in the old recording – such as high background noise,
298 physical rays on the film, and diffuse traces – severely limit the effectiveness of modern pattern recognition algorithms.
299 Consequently, the software often requires constant and thorough manual intervention by an expert operator to validate,
300 correct, or redraw the traces, making the recovery of these time series a highly labor-intensive task.

301 The present study relied on a historical dataset that represents a significant rescue of scientific heritage. Many records were
302 on obsolete 35 mm film, degraded, or even potentially flammable, and have now been digitized and standardized for
303 analysis. Similar conditions exist at other older ionospheric stations, emphasizing the importance of preserving long-term
304 ionospheric observations and fully exploiting their scientific value.

305 4 Conclusion

306 This work analyzed the response of the Concepción/Chillán ionosphere to **six** selected solar eclipses, out of a total of 21
307 identified events **(29%)** over the period 1958–2024, using a long-term historical ionogram dataset. Critical frequencies and
308 virtual heights were extracted from scaled ionograms, and regression analysis was performed to quantify the relationship
309 between solar obscuration and ionospheric parameter deviations. The study demonstrates that the E **and F1 layers** respond
310 nearly linearly to eclipse-induced reductions in solar radiation, while higher layers, particularly the F2 layer, exhibit more
311 complex and variable behavior due to additional dynamical processes. High-resolution observations, when available,
312 provided insights into short-term responses and enabled predictions for future eclipses.

313 Regression analysis focused exclusively on critical frequencies, as virtual heights often exhibited inconsistent behavior,
314 reflecting the influence of neutral winds, plasma transport, and other dynamical factors that complicate their interpretation. It
315 is important to note that only the ionospheric responses measured at Chillán during the 2 July 2019 and 14 December 2020
316 eclipses were published; no data from the remaining eclipse events have been published. The success of this study relied
317 heavily on the dedication of ionosonde operators and technicians, particularly during the 1958–1994 period, who ensured
318 frequent and reliable observations during solar eclipses. Moreover, this work represents a significant rescue of scientific
319 heritage, digitizing and standardizing records that were previously on fragile or potentially hazardous 35 mm film.
320 **Recovering decades-old analog ionogram data presents major technical challenges across three stages: (1) carefully scanning**
321 **fragile, degrading film reels; (2) digitally clipping and correcting non-linear distortions on the axes; and (3) scaling the**
322 **parameters, where heavy background noise and film damage severely limit semi-automatic software (like DISS), requiring**
323 **constant, labor-intensive manual corrections by experts.** Preserving and exploiting these long-term datasets is crucial for
324 advancing the understanding of ionospheric dynamics.

325 Predictions for the upcoming 06 February 2027 eclipse, with an expected 70% obscuration at Chillán, indicate a foE **and**
326 **foF1 decrease of 0.95 MHz ($\% \Delta f_oE = 28\%$) and 1.75 MHz ($\% \Delta f_oF1 = 24\%$), respectively,** providing a clear opportunity to
327 validate the regression models and assess their predictive skill across different solar cycle conditions.

328 **Data availability**

329 Adjusted F10.7 solar flux values were obtained from the Space Weather Services at Collecte Localisation Satellites (CLS,
330 <https://spaceweather.cls.fr/>). The SoCio code is available at <https://github.com/BenjaUP-coding/SoCio>. The *Eclipse*
331 *Calculator 2.0* application (Masana, 2012) can be found at <https://serviastro.ub.edu/en/materials/apps/eclipsi-20>. Historical
332 scaled ionospheric data during solar eclipse events are currently available at <https://11nk.dev/hklvhci>.

333

334 **Author contributions**

335 AYG: writing (original draft preparation) and data curation; MAB: Conceptualization, writing (original draft preparation)
336 and formal analysis; CAC-R: data curation; MRC: data curation; BAU: methodology and data curation; AJF: supervision
337 and validation.

338

339 **Competing interests**

340 Manuel Bravo is the guest editor of the special issue.

341

342 **Acknowledgements**

343 We are indebted to the engineers and technicians who operated the C4 and IPSS-42 ionosondes from 1957 onwards; without
344 their work, this report would not have been possible. In particular, we thank Carlos Figueroa, Herwing Herrera, José Rivera,
345 Avelino Sáez, and others. This work was supported by the Universidad Adventista de Chile, regular projects PI-175 and PI-
346 204. MAB and BAU acknowledge the ANID/SUBDIRECCIÓN DE INVESTIGACIÓN APLICADA ID25110556. **MAB**
347 **also acknowledge the ANID/FONDECYT Iniciación 11261653**. The authors acknowledge the assistance of Sider.ai in the
348 translation and preliminary review of the manuscript draft, with the subsequent and exhaustive manual scientific validation.

349 **References**

- 350 Afraimovich, E. L., Kosogorov, E. A., & Lesyuta, O. S.: Effects of the August 11, 1999 total solar eclipse as deduced from
351 total electron content measurements at the GPS network. *Journal of Atmospheric and Solar-Terrestrial Physics*,
352 64(18), 1933–1941, doi:10.1016/s1364-6826(02)00221-3, 2022.
- 353 Aryal, S., Geddes, G., Fin, S. C., Mrak, S., Galkin, I., Cnossen, I., et al.: Multi-spectral and multi instrument observation of
354 TIDs following the Total Solar Eclipse of August 21. *Journal of Geophysical Research: Space Physics*, 124, 3761–
355 3774, doi:10.1029/2018JA026333, 2019.
- 356 Bilitza, D., Pezzopane, M., Truhlik, V., Altadill, D., Reinisch, B. W., & Pignalberi, A.: The International Reference
357 Ionosphere model: A review and description of an ionospheric benchmark. *Reviews of Geophysics*, 60,
358 e2022RG000792. doi:10.1029/2022RG000792, 2022.

- 359 Bravo, M. A., Foppiano, A. J., and Abarca del Río, R.: Long-Term Dependencies of Annual and Semiannual Components of
360 NmF2 Over Concepción. *The Open Atmospheric Science Journal*, 5(1), 2-8, doi:10.2174/1874282301105010002,
361 2011.
- 362 Bravo, M., Martínez-Ledesma, M., Foppiano, A., Urra, B., Ovalle, E., Villalobos, C., Souza, J., Carrasco, E., Muñoz, P.,
363 Tamblay, L., Vega-Jorquera, P., Marín, J., Pacheco, R., Rojo, E., Leiva, R. & Stepanova, M.: First report of an eclipse
364 from Chilean ionosonde observations: comparison with total electron content estimations and the modeled maximum
365 electron concentration and its height. *J. Geophys. Res. Space Physics*, 125, e2020JA027923.
366 doi:10.1029/2020JA027923, 2020.
- 367 Bravo M.A., Molina M.G., Martínez-Ledesma M., de Haro Barbás B., Urra B., Elías A., Souza J., Villalobos C., Namour
368 J.H., Ovalle E., Venchiarutti J.V., Blunier S., Valdés-Abreu J.C., Guillermo E., Rojo E., de Pasquale L., Carrasco E.,
369 Leiva R., Castillo Rivera C., Foppiano A., Milla M., Muñoz P.R., Stepanova M., Valdivia J.A. and Cabrera M.:
370 Ionospheric response modeling under eclipse conditions: Evaluation of 14 December 2020, total solar eclipse
371 prediction over the South American sector. *Front. Astron Space Sci*, 9, doi: 10.3389/fspas.2022.1021910, 2022.
- 372 Bremer, J.: Ionospheric trends in mid-latitudes as a possible indicator of the atmospheric greenhouse effect, *Journal of*
373 *Atmospheric and Terrestrial Physics* 54, 1505-1511, 1992.
- 374 Cheng, K. H., Huang, Y. N., & Chen, S. W.: Ionospheric effects of the solar eclipse of September 23, 1987, around the
375 equatorial anomaly crest region. *Journal of Geophysical Research*, 97(A1), 103–111, doi:10.1029/91JA02409, 1992.
- 376 Chuo, Y. J.: Ionospheric effects on the F region during the sunrise for the annular solar eclipse over Taiwan on 21 May 2012,
377 *Ann. Geophys.*, 31, 1891–1898, doi:10.5194/angeo-31-1891-2013, 2013.
- 378 de Haro Barbás, BF, Bravo, M, Elías, AG, Martínez-Ledesma, M, Molina, G, Urra, B, Venchiarutti, JV, Villalobos, C,
379 Namour, JH, Ovalle, E, Guillermo, ED, Carrasco, E, de Pasquale, G, Rojo, E, Leiva R. Longitudinal variations of
380 ionospheric parameters near totality during the eclipse of December 14, 2020. *Adv. Space Res.*,
381 doi:10.1016/j.asr.2021.12.026, 2022.
- 382 Evans, J. V.: An F-region eclipse. *Journal of Geophysical Research*, 70(1), 131–142, doi: 10.1029/JZ070i001p00131, 1965a.
- 383 Evans, J. V.: On the behavior of foF2 during solar eclipses. *Journal of Geophysical Research*, 70(3), 733–738,
384 doi:10.1029/JZ070i003p00733, 1965b.
- 385 Foppiano, A.J.; Cid, L. and Jara, V.: Ionospheric long-term trends in South American mid-latitudes, *Journal of Atmospheric*
386 *and Solar-Terrestrial Physics*, 61, 717-723, 1999.
- 387 Higgs, A. J.: Ionospheric measurements made during the total solar eclipse of 1940 October 1. *Monthly Notices of the Royal*
388 *Astronomical Society*, 102(1), 24–34, doi:10.1093/mnras/102.1.24, 1942.
- 389 Hoque M.M., Wenzel, D., Jakowski, N., Gerzen, T., Berdermann, J., et al.: Ionospheric response over Europe during the
390 solar eclipse of March 20, 2015. *J. Space Weather Space Clim.*, 6, A36, doi:10.1051/swsc/2016032, 2016.
- 391 Huba, J. D., & Drob, D.: SAMI3 prediction of the impact of the 21 August 2017 total solar eclipse on the
392 ionosphere/plasmasphere system. *Geophysical Research Letters*, 44, 5928–5935. doi:0.1002/2017GL073549, 2017.

393 Jakowski, N., Stankov, S. M., Wilken, V., Borries, C., Altadill, D., Chum, J., et al.: Ionospheric behavior over Europe during
394 the solar eclipse of 3 October 2005. *Journal of Atmospheric and Solar-Terrestrial Physics*, 70(6), 836–853,
395 doi:10.1016/j.jastp.2007.02.016, 2008.

396 Jarvis, M.J., Jenkins, B., Rodgers, G.A.: Southern hemisphere observations of long-term decrease in F-region altitude and
397 thermospheric wind providing possible evidence for global thermospheric cooling, *Journal of Geophysical Research*,
398 103, 20774-20787, 1998.

399 Kumar, S., Singh, A. K., & Singh, R. P.: Ionospheric response to total solar eclipse of 22 July 2009 in different Indian
400 regions. *Annales de Geophysique*, 31(9), 1549–1558, doi:10.5194/angeo-31-1549-2013, 2013.

401 Lastovicka, J.: Progress in investigating long-term trends in the mesosphere, thermosphere, and ionosphere, *Atmos. Chem.*
402 *Phys.*, 23, 5783–5800, doi:10.5194/acp-23-5783-2023, 2023.

403 Laštovicka, J., Solomon, S.C. and Qian, L.: Trends in the Neutral and Ionized Upper Atmosphere, *Space Sci Rev*,
404 doi:10.1007/s11214-011-9799-3, 2017.

405 Le, H., Liu, L., Yue, X., and Wan, W.: The ionospheric responses to the 11 August 1999 solar eclipse: observations and
406 modeling, *Ann. Geophys.*, 26, 107–116, doi:10.5194/angeo-26-107-2008, 2008.

407 Le, H., Liu, L., Yue, X., Wan, W., and Ning B.: Latitudinal dependence of the ionospheric response to solar eclipses, *J.*
408 *Geophys. Res.*, 114, A07308, doi:10.1029/2009JA014072, 2009.

409 Lei, J., Dang, T., Wang, W., Burns, A., Zhang, B., & Le, H.: Long-lasting response of the global thermosphere and
410 ionosphere to the 21 August 2017 solar eclipse. *Journal of Geophysical Research: Space Physics*, 123, 4309–4316,
411 doi:10.1029/2018JA025460, 2018.

412 Martínez-Ledesma, M., Bravo, M., Urra, B., Souza, J., and Foppiano, A.: Prediction of the ionospheric response to the 14
413 December 2020 total solar eclipse using SUPIM-INPE. *JGR. Space Phys.* 125, e2020JA028625.
414 doi:10.1029/2020JA028625, 2020.

415 Masana, E.: Eclipsi 2.0 (Eclipse Calculator 2.0) [Mobile application software]. ServiAstro — Universitat de Barcelona.
416 Available in: <https://serviastro.ub.edu/en/materials/apps/eclipsi-20>, 2012.

417 Mitra, S. K., Rakshit, H., Syam, P., & Ghose, B. N.: Effect of the solar eclipse on the ionosphere. *Nature*, 132(3333), 442–
418 443. doi:10.1038/132442a0, 1933.

419 Momani, M. A., Yatim, B., & Mohd Ali, M. A.: Ionospheric and geomagnetic response to the total solar eclipse on 1 August
420 2008 over Northern Hemisphere. *Journal of Geophysical Research*, 115, A08321, doi:10.1029/2009JA014999, 2010.

421 Muzzioli, L.: La Estación de la Ionósfera, Atenea No. 435, 1er Semestre, 179-191, 1977.

422 Ortiz de Adler, N., Elías, A.G., Manzano, J.R.: Solar cycle length variations: its relation with ionospheric parameters.
423 *Journal of Atmospheric and Terrestrial Physics* 59, 159-162, 1997.

424 Ovalle E. M., Villalobos C. U., Agüero L. A., Leiva R. E., Foppiano A. J.: A new ionospheric station for Chile, *Bulletin No*
425 74, Ionospheric Network Advisory Group, Union Radio Scientific Internationale, 2017.

426 Pezzopane, M., Pietrella, M., Pignalberi, A., & Tozzia, R.: 20 March 2015 solar eclipse influence on sporadic E layer.
427 *Advances in Space Research*, 56(10), 2064–2072, doi:10.1016/j.asr.2015.08.001, 2015.

428 Piggott, W. R. & Rawer, K.: U.R.S.I. Handbook of Ionogram Interpretation and Reduction. U.S. Department of Commerce
429 National Oceanic and Atmospheric Administration-Environmental Data Service, Asheville, North Carolina, USA,
430 326 pp., 1972.

431 Ramírez, P.M.: Física de la ionósfera e interpretación de los ionogramas obtenidos en la Estación Concepción, como
432 colaboración al Año Geofísico Internacional, Facultad de Ingeniería, Universidad de Concepción, 1963.

433 Ratcliffe, J. A.: A survey of solar eclipses and the ionosphere. In W. J. G. Beynon & G. M. Brown (Eds.), *Solar eclipses and*
434 *the ionosphere* (pp. 1–13). Oxford: Pergamon Press, 1956.

435 Reinisch, B. W., Dandenaault, P. B., Galkin, I. A., Hamel, R., & Richards, P. G.: Investigation of the electron density
436 variation during the 21 August 2017 solar eclipse. *Geophysical Research Letters*, 45, 1253–1261, doi:
437 10.1002/2017GL076572, 2018.

438 Rishbeth, H.: Solar eclipses and ionospheric theory. *Space Science Reviews*, 8(4), 543–554. doi:10.1007/BF00175006, 1968.

439 Smith, P.A., King, J.W.: Long-term relationships between sunspots, solar faculae and the ionosphere. *Journal of*
440 *Atmospheric and Terrestrial Physics* 43, 1057-1063, 1981.

441 Urra, B.: SoCio, Software de Corrección de Ionogramas , <https://github.com/BenjaUP-coding/SoCio>, 2026.

442 Zhang, H., Zhang, T., Zhang, X., Yuan, Y., Wang, Y., & Ma, Y.: Multi-Instrument Observations of the Ionospheric
443 Response Caused by the 8 April 2024 Total Solar Eclipse. *Remote Sensing*, 16(13), 2451, doi:10.3390/rs16132451,
444 2024.